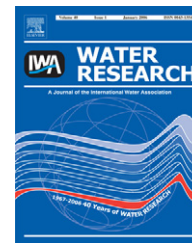


Available at www.sciencedirect.comjournal homepage: www.elsevier.com/locate/watres

A computational model for biofilm-based microbial fuel cells

Cristian Picioreanu^{a,*}, Ian M. Head^c, Krishna P. Katuri^b, Mark C.M. van Loosdrecht^a, Keith Scott^b

^aDepartment of Biotechnology, Faculty of Applied Sciences, Delft University of Technology, Julianalaan 67, 2628 BC Delft, The Netherlands

^bSchool of Chemical Engineering and Advanced Materials, University of Newcastle Upon Tyne, Merz Court, Newcastle Upon Tyne, Tyne & Wear NE1 7RU, UK

^cSchool of Civil Engineering and Geosciences, University of Newcastle Upon Tyne, Devonshire Building, Newcastle Upon Tyne, Tyne & Wear NE1 7RU, UK

ARTICLE INFO

Article history:

Received 26 October 2006

Received in revised form

11 April 2007

Accepted 12 April 2007

Available online 29 May 2007

Keywords:

Microbial fuel cell

Mathematical model

Biofilm

Redox mediator

Electricity

ABSTRACT

This study describes and evaluates a computational model for microbial fuel cells (MFCs) based on redox mediators with several populations of suspended and attached biofilm microorganisms, and multiple dissolved chemical species. A number of biological, chemical and electrochemical reactions can occur in the bulk liquid, in the biofilm and at the electrode surface. The evolution in time of important MFC parameters (current, charge, voltage and power production, consumption of substrates, suspended and attached biomass growth) has been simulated under several operational conditions. Model calculations evaluated the effect of different substrate utilization yields, standard potential of the redox mediator, ratio of suspended to biofilm cells, initial substrate and mediator concentrations, mediator diffusivity, mass transfer boundary layer, external load resistance, endogenous metabolism, repeated substrate additions and competition between different microbial groups in the biofilm. Two- and three-dimensional model simulations revealed the heterogeneous current distribution over the planar anode surface for younger and patchy biofilms, but becoming uniform in older and more homogeneous biofilms. For uniformly flat biofilms one-dimensional models should give sufficiently accurate descriptions of produced currents. Voltage- and power-current characteristics can also be calculated at different moments in time to evaluate the limiting regime in which the MFC operates. Finally, the model predictions are tested with previously reported experimental data obtained in a batch MFC with a *Geobacter* biofilm fed with acetate. The potential of the general modeling framework presented here is in the understanding and design of more complex cases of wastewater-fed microbial fuel cells.

© 2007 Elsevier Ltd. All rights reserved.

1. Introduction

Research on microbial fuel cells (MFCs) is at present receiving a striking increase in interest because these devices can

directly convert a large diversity of organic compounds into electricity (see several recent reviews by Shukla et al., 2004; Chang et al., 2006; Lovley, 2006; Katz et al., 2003; Bullen et al., 2005; Rabaey et al., 2005a; Rabaey and Verstraete, 2005; Logan

*Corresponding author. Tel.: +31 15 2781166; fax: +31 15 2782355.

E-mail addresses: C.Picioreanu@tudelft.nl (C. Picioreanu), i.m.head@ncl.ac.uk (I.M. Head), k.p.katuri@ncl.ac.uk (K.P. Katuri), M.C.M.vanLoosdrecht@tudelft.nl (M.C.M. van Loosdrecht), k.scott@ncl.ac.uk (K. Scott).

0043-1354/\$ - see front matter © 2007 Elsevier Ltd. All rights reserved.

doi:10.1016/j.watres.2007.04.009

Nomenclature	
A	area, L^2
b	Tafel coefficient, $L^2MT^{-3}I^{-1}$ (e.g., V)
d	density, ML^{-3}
D	diffusion coefficient, L^2T^{-1}
E	equilibrium potential, $L^2MT^{-3}I^{-1}$ (e.g., V)
F	Faraday's constant (96,480 C/mol e^-)
ΔG	Gibbs energy, L^2MT^{-2} (e.g., kJ)
i	current density, IL^{-2}
I	total current through the MFC, I
K	half-saturation coefficient, NL^{-3} or ML^{-3}
K_a	acidity constant
L	dimension in biofilm domain, L
m	mass of biomass particles, M
n	number of moles, N
P	microbial fuel cell power, L^2MT^{-3} (e.g., W)
Q	total charge produced, TI (e.g., C)
q	specific rate, $MM^{-1}T^{-1}$
r	net reaction rate at electrode, $ML^{-2}T^{-1}$ or $NL^{-2}T^{-1}$ or in bulk or biofilm, $ML^{-3}T^{-1}$ or $NL^{-3}T^{-1}$
R	electrical resistance, $L^2MT^{-3}I^{-2}$ (e.g., Ω)
S	dissolved chemical component (solute) concentration, NL^{-3} or ML^{-3}
t	time, T
V	voltage (for the MFC) or potential (for the electrodes), $L^2MT^{-3}I^{-1}$ (e.g., V)
v	volume, L^3
X	biomass component (particulate) concentration, ML^{-3}
x, y, z	coordinates in the biofilm (z perpendicular to the electrode surface), L
Y	yield, N/N or M/M
γ	degree of reduction for a dissolved or biomass compound (e^-/C -mol)
Φ	volumetric flowrate, L^3T^{-1}
η	overpotential (or polarization potential), $L^2MT^{-3}I^{-1}$ (e.g., V)
ρ	absolute reaction rate, $ML^{-3}T^{-1}$
Subscripts	
0	initial
A	anode
Ac	acetate
ata	attachment
B	bulk liquid
C	cathode
CAT	catabolic reaction
Car	carbonate
cell	microbial fuel cell
conc	concentration
det	detachment
e	calculated per mol electron
E	electrode
ext	external electrical circuit of MFC
F	biofilm
G	Gibbs energy
H	hydrogen ion (H^+)
i	index of a solute or biomass component
int	internal electrical circuit of MFC
j	index of a reaction
L	boundary layer
M	mediator (general form)
Met	methanogen
Mox	oxidized mediator (M)
Mred	reduced mediator (MH_2)
ohm	ohmic
Q	coulombic (charge)
ref	reference
S	soluble component
X	biomass
Superscripts	
01	biochemical reference conditions, but with pH 7
0	standard reference conditions (1 mol/L, 1 atm, 298 K)
[B]	reference to concentrations in bulk liquid
max	maximum
Note:	
L, M, T, I and N are the dimensions of the quantities length, mass, time, electric current, and amount of substance, respectively. The units of all model variables are in Tables 1–3.	

et al., 2006). However, multiple physical, chemical and biological factors interact and play a role in determining final MFC performance. This complicates the analysis of a MFC system, which requires an inherently multidisciplinary approach if in-depth understanding of how they function is to be achieved. Although in the field of chemical fuel cells mathematical models are highly developed and widely used (e.g., *Fuel Cell Handbook*, 2004), to date work on MFC has been mainly experimental. Current research (Schubert, 2006) is oriented either towards understanding the microbiology of electrochemically active microorganisms (Stams et al., 2006)

or to the engineering and design of ever more efficient and versatile MFCs (for example, Rabaey et al., 2003; Liu and Logan, 2004). It is our conviction however that, if rationally constructed and used, mathematical models can be useful to both microbiologists and engineers. This is because almost all aspects of the MFC operation can be regarded as sub-optimal at this point, including the anode, the cathode, the membrane, and MFC design (Chang et al., 2006). For engineers, mathematical models can help to detect rate-limiting steps and to allow the development of strategies to improve the MFC's design and power output. Biologists on the other hand

can use computational models to test hypotheses about microbial community composition, size, activity and modes of electron transfer in MFCs or to design new experiments. Moreover, the computational models help by pointing to the most important MFC parameters that should be experimentally measured and reported.

The information available at present is restricted to simple calculations of overall coulombic end energy efficiency, overall growth yield, maximum attainable power and open circuit potential (Rabaey et al., 2005b; Logan et al., 2006; Menicucci et al., 2006). An isolated exception is a preliminary model for MFC with suspended cells and added redox mediator (Zhang and Halme, 1995). Surprisingly, this line of research has not been pursued further, and the evolution in time of MFC parameters (current, voltage and power production, consumption of substrates, suspended and attached biomass growth) in a biofilm-based MFC has not been previously described by any reported model.

This report therefore has the main goal of laying the basis of a general model describing MFC behavior with both suspended and attached cells in the form of biofilms. Since this is the first attempt of its kind, we shall focus here only on electron transfer from microbial cells to the anode via an added diffusible mediator. Including other electron transfer mechanisms such as by an endogenously generated mediator, by direct contact (Chang et al., 2006), or connection to the anode via proposed conducting structures termed “nanowires” (Reguera et al., 2005) in the model framework is possible, and shall be presented in further studies. In this model, we aim to describe in detail only the dynamic behavior of the anodic compartment, having in mind that a description of the cathodic chamber can follow the same approach. This study also evaluates the model performance in several scenarios involving both cells in suspension and cells in biofilms developed on the anode of a MFC.

2. Model description

A goal of any mathematical model of a microbial fuel cell is to, at least, calculate the electrical current and voltage generated. The electrical current occurs when certain dissolved chemical species are oxidized on the anode and others are reduced on the cathode. A first task consists of defining an electrochemical model for the electrode reactions, which depend on the electrode potential and on concentrations of reactants/products at the electrode surface. Secondly, because the concentrations of chemical and biomass components are determined by the mass transport and reactions in the biofilm and bulk liquid, a previously described biofilm model using mass balances is incorporated in a slightly adapted form (Picioreanu et al., 2004; Xavier et al., 2005).

The general model is implemented in computer software written in C/C++. An easy to use text-based input file provides a modeling framework in which any number of soluble components and biomass types together with their relevant physical, chemical and biological attributes can be defined. Electrochemical and (bio)chemical reactions can also be defined based on their stoichiometry and rate parameters. One-, two- or three-dimensional descriptions of the biofilm

system can be alternatively chosen. A model scheme (Fig. S1) and solution algorithm (Fig. S2) are presented in the Supplementary Material. For the standard case reported in this article (case no. 1), a simulation of 15 days MFC operation with time steps of 0.5 h takes ~6 min (one-dimensional, 1d), ~30 min (two-dimensional, 2d) or ~14 h (three-dimensional, 3d) on a PC (2.6 GHz processor).

The model is applied here for the particular case of a MFC fed with acetate, operated in batch mode. Acetate is chosen in the examples as substrate because its complete degradation to CO₂ follows a simpler pathway than substrates with higher numbers of carbons (e.g., glucose, butyrate, etc.). It is also assumed that a certain concentration of redox mediator exists from the beginning in the bulk liquid.

2.1. Electrochemical model

2.1.1. Electrode rates

The rate for the electrochemical oxidation of a reduced mediator at the anode surface



is expressed as a function of current density as

$$r_{M_{\text{red}},E} = -\frac{i}{2F}, \quad r_{M_{\text{ox}},E} = \frac{i}{2F}. \quad (2)$$

The current density produced in the electrochemical mediator oxidation is represented by the Butler–Volmer equation (see, for example, Newman, 1991, pp. 188–190)

$$i = i_{0,\text{ref}} \left(\frac{S_{E,M_{\text{red}}}}{S_{\text{ref},M_{\text{red}}}} \right) \left(\frac{S_{E,M_{\text{ox}}}}{S_{\text{ref},M_{\text{ox}}}} \right)^{-1} \left(\frac{S_{E,H}}{S_{\text{ref},H}} \right)^{-2} \times \left[\exp\left(\frac{2.303}{b} \eta_{\text{act}}\right) - \exp\left(-\frac{2.303}{b} \eta_{\text{act}}\right) \right]. \quad (3)$$

All concentrations S_E in Eq. (3) are at the electrode surface. These concentrations are also used to calculate the activation overpotential η_{act} .

2.1.2. Current and charge

The current I collected at an electrode is obtained by integration of all possible local current densities i_j over the electrode surface (as in the biofilm-induced biocorrosion model of Picioreanu and Van Loosdrecht, 2002)

$$I = \int_{A_F} \sum_j i_j \, dA. \quad (4)$$

The problem is however complicated by the fact that Eq. (4) is implicit in I : the activation overpotential, which is the driving force for the current density i_j , depends in turn on the current I . A potential balance over the MFC permits calculation of the activation overpotential as is explained in Section 2.1.3 (see also the solution method in Supplementary Material). The charge (Coulombs) produced is calculated from the integration of cell current over time

$$Q = \int_0^t I \, dt. \quad (5)$$

The coulombic yield (Y_Q) is the ratio between the actual charge produced Q and the maximum theoretical one, Q_{max} , which is the number of electrons (γ) available for a redox reaction in all oxidizable substrates (n_i moles) fed to

the fuel cell

$$Y_Q = \frac{Q}{Q_{\max}} = \frac{Q}{\sum_i \gamma_i n_i} \quad (6)$$

2.1.3. Voltage and overpotential

When the (microbial) fuel cell is connected with an external resistance R_{ext} (also called “load”), Ohm’s law $V_{\text{cell}} = IR_{\text{ext}}$ gives the microbial fuel cell voltage, V_{cell} . Furthermore, the cell power is $P = V_{\text{cell}}I$. The actual fuel cell voltage is decreased from the equilibrium potential, E_{cell} (the maximum imposed by thermodynamics), by a series of irreversible losses $V_{\text{cell}} = E_{\text{cell}} - \text{Losses}$. The equilibrium cell potential E_{cell} is expressed by the difference between the ideal equilibrium potentials of the cathode and anode, $E_C^{(B)}$ and $E_A^{(B)}$, respectively. The $E_C^{(B)}$ and $E_A^{(B)}$ at a moment in time are calculated as a function of the concentrations of reacting chemical species in the bulk liquid, S_B , at that moment.

The losses, called overpotential or polarization, originate primarily from three sources: (1) activation overpotential (η_{act} , related to the rates of electrode reactions), (2) ohmic overpotential (η_{ohm} , related to the resistance to the flow of ions in the electrolyte and to flow of electrons through the electrode materials), and (3) concentration overpotential (η_{conc} , related to mass transfer limitations of chemical species transported to or from the electrode). All these overpotentials are by convention here positive values.

By summation of all polarization losses, the cell voltage is written as

$$V_{\text{cell}} = (E_C^{(B)} - E_A^{(B)}) - (\eta_{\text{act}} + \eta_{\text{ohm}} + \eta_{\text{conc}}) \quad (7)$$

The activation and concentration overpotentials occur separately both at cathode and anode, so that one obtains

$$V_{\text{cell}} = (E_C^{(B)} - \eta_{C,\text{act}} - \eta_{C,\text{conc}}) - (E_A^{(B)} + \eta_{A,\text{act}} + \eta_{A,\text{conc}}) - \eta_{\text{ohm}} \quad (8)$$

Concentration overpotentials will correct the ideal equilibrium electrode potentials taking into account that the actual concentrations at the electrochemical reaction site are the concentrations S_E at the electrode surface. Concentrations S_E are determined by mass transport and reaction and are variable in time (and for 2d or 3d models also in space). If, for a reactant, the difference in concentration between bulk and electrode surface creates the concentration polarization $\eta_{\text{conc}} = RT/(nF)\ln(S_E/S_B)$ (Fuel Cell Handbook, 2004), then we can define new equilibrium potentials for the cathode and anode, E_C and E_A , as a function of S_E . If both the electrolyte and fuel cell electrodes obey Ohm’s law, then $\eta_{\text{ohm}} = IR_{\text{int}}$. One can therefore write Eq. (8) as

$$V_{\text{cell}} = (E_C - \eta_{C,\text{act}}) - (E_A + \eta_{A,\text{act}}) - IR_{\text{int}} \quad (9)$$

For simplification, because the model focuses on the behavior of the anodic chamber, a constant value for the cathode potential, $V_C = E_C - \eta_{C,\text{act}}$, is assumed. Values for the equilibrium potentials of all anodic reactions are needed, as functions of the standard redox potential, amended for the actual concentrations calculated at the electrode surface. For example, the mediator oxidation reaction (1) has

$$E_M = E_M^0 + \frac{RT}{2F} \ln \frac{S_{M_{\text{ox}}} S_{H^+}^2}{S_{M_{\text{red}}}} \quad (10)$$

Finally, at 25 °C, with the internal and external resistances known, with the standard reduction potential E_M^0 for the mediator couple, and with $V_{\text{cell}} = IR_{\text{ext}}$, the activation overpotential is

$$\eta_{\text{act}} = V_C - I(R_{\text{int}} + R_{\text{ext}}) - \left(E_M^0 - 0.059 \text{pH} + \frac{0.059}{2} \log \frac{S_{E,M_{\text{ox}}}}{S_{E,M_{\text{red}}}} \right) \quad (11)$$

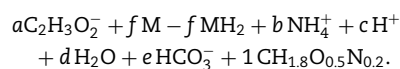
Consequently, it is necessary to know the concentrations S_E of electroactive species at the electrode surface. These concentrations are determined by the rates of diffusion through a mass transfer boundary layer and through the biofilm growing on the electrode, in combination with all reactions occurring in the biofilm and on the electrode. The rigorous way to find these concentrations is by solving a set of mass balances in the biofilm and bulk liquid domains, which will be explained in the following sections.

2.2. Biofilm/bulk liquid model

2.2.1. Microbial reaction stoichiometry

In general, the reaction stoichiometry of microbial growth relates the amounts of different substrates consumed to the amounts of metabolic products and biomass formed during a certain microbial conversion. In order to construct a realistic model for the biotransformations occurring in the MFC, it is essential to have the reaction stoichiometry based not only on correct elemental and charge balances, but also on the second law of thermodynamics.

Microorganisms from MFC extract the large quantities of Gibbs free energy needed to build biomass (the anabolic process) from redox reactions (catabolism) involving an electron donor/electron acceptor couple. We shall assume for the purposes of this example that the MFC bacteria grow anaerobically on acetate as electron donor and carbon source, with oxidized mediator as electron acceptor, and with NH_4^+ as N source. The growth system contains acetate, biomass (with a typical elemental formula $\text{CH}_{1.8}\text{O}_{0.5}\text{N}_{0.2}$, cf. Heijnen, 1999), oxidized mediator ($M_{\text{ox}} \equiv M$), reduced mediator ($M_{\text{red}} \equiv \text{MH}_2$), HCO_3^- , NH_4^+ , H^+ and H_2O as the eight relevant components. The general macro-chemical reaction equation for the production of 1 C-mol biomass can be written as



The six stoichiometric coefficients (a–f) can be calculated from the conservation equations for C, H, O, N, electric charge, and the Gibbs energy balance. Because we may not always know the Gibbs energy of formation for the mediator species, we adopt the approach of Heijnen (1999), based on the Gibbs energy per electron present in the redox couple, ΔG_e^{01} . This has the advantage of being directly related (by $\Delta G_e^{01} = -FE^{01}$) to the conventional redox potential of redox half reactions, E^{01} , which is normally known for a given mediator. ΔG_e^{01} is calculated at biochemical standard conditions (pH 7, 298K, 1mol/L, 1bar), using HCO_3^- , the most abundant form of carbon dioxide at this pH.

First, the Gibbs energy of the catabolic reaction ΔG_{CAT} is calculated from the Gibbs energies of half-reactions

$$-\Delta G_{\text{CAT}} = \gamma_{\text{Ac}} \left(\Delta G_{\text{e,Ac}}^{01} - \Delta G_{\text{e,M}}^{01} \right). \quad (12)$$

For the acetate/ HCO_3^- couple (electron donor), $\Delta G_{\text{e,Ac}}^{01} = 26.8 \text{ kJ/e-mol}$ (Table 3 from Heijnen, 1999). For the mediator couple (electron acceptor), $\Delta G_{\text{e,M}}^{01} = -FE_M^{01}$. Taking thionine as mediator in this example, the reduction potential at biochemical standard is $E_M^{01} = 0.064 \text{ V}$ (Roller et al., 1984) (that is, $E_M^0 = 0.477 \text{ V}$ in standard conditions, vs. standard hydrogen electrode, SHE), thus $\Delta G_{\text{e,M}}^{01} = -6.175 \text{ kJ/e-mol}$. The reduction degree for acetate is $\gamma_{\text{Ac}} = 4 \text{ e/C-mol}$, thus $-\Delta G_{\text{CAT}} = 131.9 \text{ kJ/C-molAc}$.

Second, the dissipated Gibbs energy can be estimated from a correlation function of the number of carbon atoms in the electron donor and its degree of reduction (Heijnen, 1999). If maintenance is neglected, the estimated maximum energy dissipation yield is $1/Y_{\text{GX}}^{\text{max}} = 432 \text{ kJ/C-mol biomass}$.

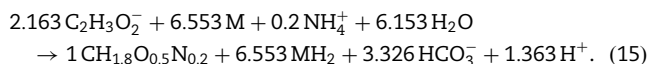
Finally, from a balance of degree of reduction (conservation of electrons) and the Gibbs energy balance, and with a degree of reduction for biomass $\gamma_X = 4.2$, the maximum yield of C-mol biomass/C-mol acetate, $Y_{\text{Ac,X}}^{\text{max}}$, is (Heijnen, 1999)

$$Y_{\text{Ac,X}}^{\text{max}} = \frac{(-\Delta G_{\text{CAT}})}{\frac{1}{Y_{\text{GX}}^{\text{max}}} + \frac{\gamma_X}{\gamma_{\text{Ac}}} (-\Delta G_{\text{CAT}})} = 0.231 \text{ C-mol biomass/C-mol acetate}, \quad (13)$$

which means a stoichiometric coefficient $a = -2.163 \text{ mol acetate/C-mol biomass}$. In a similar manner, the yield of biomass from mediator (with $\gamma_M = -2$ because two electrons are involved per mol thionine) can be calculated as (Heijnen, 1999)

$$Y_{\text{MX}}^{\text{max}} = \frac{\frac{-\gamma_M}{\gamma_{\text{Ac}}} (-\Delta G_{\text{CAT}})}{\frac{1}{Y_{\text{GX}}^{\text{max}}}} = 0.153 \text{ C-mol biomass/mol mediator}, \quad (14)$$

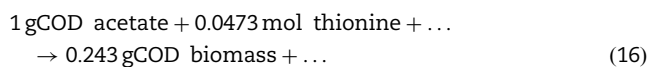
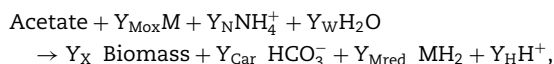
which gives the stoichiometric coefficient $f = -6.553 \text{ mol mediator/C-mol biomass}$. The rest of four stoichiometric coefficients follow from the elemental and charge balances. The calculated molar stoichiometry of microbial growth on acetate with thionine as electron acceptor is



In wastewater treatment, the biomass yield is calculated on chemical oxygen demand (COD) basis. In terms of COD, the maximum biomass yield is

$$Y_X = \frac{\gamma_X}{\gamma_{\text{Ac}}} Y_{\text{Ac,X}}^{\text{max}} = 0.243 \text{ gCOD biomass/gCOD acetate}.$$

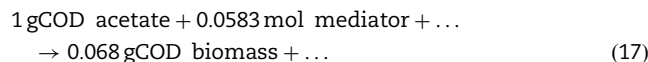
The reaction stoichiometry per gCOD acetate is therefore



Y_{N} and Y_{W} are neglected. The remaining calculated yields per gCOD acetate consumed are listed in Table 1.

A hypothetical mediator with a lower reduction potential would theoretically give a higher coulombic yield. However,

for microbial growth this is energetically less favorable and less biomass would be produced. For example, one can calculate that for $E_M^{01} = -0.200 \text{ V}$ (that is, $E_M^0 = 0.210 \text{ V}$ in standard conditions, vs. SHE), the Gibbs energy produced in catabolism is only $-\Delta G_{\text{CAT}} = 30 \text{ kJ/C-molAc}$. With this value, one obtains only $0.068 \text{ gCOD biomass/gCOD acetate}$



As it will be shown by model simulations, although in a pure culture, the lower-potential mediator produces more electrons per substrate (has a higher coulombic yield), in a mixed culture this too slow-growing microorganism can potentially not compete with others having a higher growth rate.

2.2.2. Microbial reaction kinetics

The absolute rate of acetate conversion with oxidized mediator leading to microbial growth can be expressed as a double Monod limitation kinetic equation (standard parameters in Table 1)

$$\rho = q_{\text{Ac,max}} X \frac{S_{\text{Ac}}}{K_{\text{Ac}} + S_{\text{Ac}}} \frac{S_{\text{Mox}}}{K_{\text{Mox}} + S_{\text{Mox}}}. \quad (18)$$

The net rates for acetate, biomass, the two mediator forms, bicarbonate and protons are expressed using rate Eq. (18) and the stoichiometric Eq. (16) as

$$r_{\text{Ac}} = -\rho, \quad r_X = Y_X \rho, \quad r_{\text{Mred}} = Y_{\text{M}} \rho, \\ r_{\text{Mox}} = -Y_{\text{M}} \rho, \quad r_{\text{Car}} = Y_{\text{Car}} \rho, \quad r_{\text{H}} = Y_{\text{H}} \rho. \quad (19)$$

The rates (19) are applied in mass balances for components in biofilm (with $S_{\text{F,Ac}}$, $S_{\text{F,Mox}}$, $S_{\text{F,Mred}}$, $S_{\text{F,Car}}$, $S_{\text{F,H}}$ and X_{F} all variable in time and space) as well as in the bulk liquid (with $S_{\text{B,Ac}}$, $S_{\text{B,Mox}}$, $S_{\text{B,Mred}}$, $S_{\text{B,Car}}$, $S_{\text{B,H}}$ and X_{B} all variable in time).

2.2.3. Mass balances in bulk liquid

The bulk liquid in the anodic compartment of a MFC will be considered completely mixed so that solute and biomass concentrations, S_{B} and X_{B} , (and accordingly their local reaction rates) can be assumed uniform in the whole bulk liquid.

Soluble components: A system of n_s ordinary differential equations representing mass balances of each soluble component (chemical species) in the bulk liquid will be solved

$$\frac{dS_{\text{B}}}{dt} = \frac{\Phi}{V_{\text{B}}} (S_{\text{in}} - S_{\text{B}}) + r_{\text{S,B}} + \frac{1}{V_{\text{B}}} \int_{V_{\text{F}}} r_{\text{S,F}} dV + \frac{1}{V_{\text{B}}} \int_{A_{\text{F}}} r_{\text{S,E}} dA \quad (20)$$

with a set of specified initial conditions $S_{\text{B}}(t=0) = S_0$ for all soluble components. Mass balances (20) take into account rates of exchange with the exterior and the rates of reactions in the bulk, in the biofilm and on the electrode. In the model case study chosen as an example, batch operation is assumed ($\Phi = 0$), but continuous operation can also be simulated. The net rates of reaction in the bulk ($r_{\text{S,B}}$) and in the biofilm ($r_{\text{S,F}}$) are made up of contributions from rates ρ_i of all individual reactions i multiplied by the corresponding stoichiometric coefficients (or 'yields' in biotechnological applications). These rates are given by Eq. (19). The rate of exchange between the biofilm and bulk liquid can be expressed in one of two ways: (1) as the product between an average mass flux of component to/from the biofilm, $\bar{j}_{\text{S,F}}$ ($\text{kg/m}^2 \text{ s}$ or $\text{kmol/m}^2 \text{ s}$), and the surface area of the biofilm A_{F} (m^2) or (2) an average

Table 1 – Model parameters for the standard case simulation with biofilm developing on the anode of a batch MFC fed with acetate

Parameter	Description	Value	Units
<i>Dissolved components</i>			
$S_{0,Ac}$	Initial concentration substrate (acetate)	100	gCOD m ⁻³
$S_{0,Mred}$	Initial concentration reduced mediator	10 ⁻³	mM
$S_{0,Mox}$	Initial concentration oxidized mediator	1	mM
$S_{0,Car}$	Initial concentration bicarbonate	20	mM
$S_{0,Na}$	Initial concentration cations (Na ⁺) ^a	17.8	mM
D_{Ac}	Diffusion coefficient substrate (acetate) ^b	6.5 × 10 ⁻⁶	m ² day ⁻¹
D_{Mred}, D_{Mox}	Diffusion coefficient mediator	2 × 10 ⁻⁶	m ² day ⁻¹
D_{Car}	Diffusion coefficient bicarbonate ^b	1.7 × 10 ⁻⁶	m ² day ⁻¹
D_{Na}	Diffusion coefficient cations (Na ⁺) ^b	1.16 × 10 ⁻⁶	m ² day ⁻¹
$K_{a,Ac}$	Acidity constant acetate ^b	10 ^{-4.757}	
$K_{a,Car}$	Acidity constant bicarbonate ^b	10 ^{-6.352}	
L_L	Mass transfer boundary layer thickness	10	μm
<i>Biomass components</i>			
X_0	Initial biomass concentration in bulk liquid	0.01	gCOD m ⁻³
n_{p0}	Initial number of biomass particles	5 (2d case) 165 (3d case)	Particles
d_x	Density of biomass particles ^c	300000	gCOD m ⁻³
m_0	Initial mass of biomass particles ^c	10 ⁻¹²	gCOD
$m_{X,max}$	Critical biomass for biomass particle division ^c	2 × 10 ⁻¹²	gCOD
<i>System dimensions</i>			
V_B	Bulk liquid volume	2.5 × 10 ⁻⁴	m ³
A_F	Anode surface area	10 ⁻³	m ²
$L_X \times L_Y \times L_Z$	Size of biofilm computational domain	66 × 66(× 66)	μm × μm(× μm)
$N \times M \times L$	Number of grid nodes in x, y (and z) for biofilm space discretization in 2d and 3d	33 × 33(× 33)	Nodes
<i>Electrical parameters</i>			
V_C	Cathode potential	0.68	V (SHE)
$R_{int}+R_{ext}$	Total cell resistance	100	Ω
<i>Electrochemical rate parameters</i>			
$i_{0,ref}$	Exchange current density for mediator oxidation in reference conditions ($S_{ref,Mred} = S_{ref,Mox} = 1$ mM, $S_{ref,H+} = 10^{-7}$ M)	2 × 10 ⁻⁴	A m ⁻²
E_M^0	Standard reduction potential for the mediator couple (vs. SHE) ^d	0.477	V (SHE)
b	Tafel coefficient for mediator oxidation ^e	0.120	V
<i>Microbial rate parameters</i>			
$q_{Ac,max}$	Maximum specific rate constant for microbial consumption of acetate ^f	10	(gCOD acetate) (gCOD biomass) ⁻¹ day ⁻¹
K_{Ac}	Monod half-saturation coefficient for substrate acetate ^f	100	gCOD m ⁻³
K_{Mox}	Monod half-saturation coefficient for oxidized mediator	0.1	mM
Y_X	Yield biomass on substrate ^g	0.243	(gCOD biomass) (gCOD acetate) ⁻¹
Y_{Mox}, Y_{Mred}	Yield mediator vs. substrate ^g	0.0473	(mol mediator) (gCOD acetate) ⁻¹
Y_{Car}	Yield bicarbonate from substrate ^g	0.024	(mol HCO ₃ ⁻) (gCOD acetate) ⁻¹
Y_H	Yield protons from substrate ^g	0.0098	(mol H ⁺) (gCOD acetate) ⁻¹

Values for the other model parameters were assumed based on common practical experience.

^a Calculated from charge balance to yield pH ≈ 7.

^b As in Batstone et al. (2004).

^c Similar to Picioreanu et al. (2004) and Xavier et al. (2005).

^d From Roller et al. (1984), at pH 0.

^e Assumed for a two-electron reaction.

^f From Batstone et al. (2002).

^g Calculated from a thermodynamic approach based on Heijnen (1999).

rate of reaction in the biofilm $\bar{r}_{S,F}$ (kg/m³s or kmol/m³s) times the biofilm volume, V_F (m³)

$$\bar{j}_{S,F}A_F = \bar{r}_{S,F}V_F = \int_{V_F} r_{S,F} dV. \quad (21)$$

The second option was preferred, because the change in the volumetric rates of solute components can be easily calculated. A second reason is that in a 2d or 3d model case the biofilm surface is actually not the same as the electrode area on which the biofilm is supported and therefore not easily known. Similarly, the electrochemical rates of solute component change on the electrode surface, $r_{S,E}$ (given by Eq. (2)) can be integrated over the electrode surface to give the contribution of the surface reactions to solute accumulation. The solution of Eqs. (20) is a set of bulk liquid concentrations needed at each moment in time as boundary conditions for solute mass balances in the biofilm.

Biomass components: Similar to the solute balances, mass balances are also written for all n_x relevant biomass types included in the model

$$\frac{dX_B}{dt} = \frac{\phi}{V_B}(X_{in} - X_B) + r_{X,B} + r_{det} \frac{A_F}{V_B} - r_{ata} \frac{A_F}{V_B}. \quad (22)$$

Initial concentrations of all biomass types suspended in the bulk liquid, X_0 , need to be assumed in accordance with those used in the experiments. In the batch case exemplified here, $\phi = 0$. Moreover, for simplicity, the biomass exchange between bulk and biofilm (the surface-based rates of biomass detachment and attachment) has been ignored in the case studies presented here although the general model implementation offers this possibility.

2.2.4. Mass balances in biofilm

Unlike the bulk liquid, the biofilm sub-domain is characterized by spatial concentration gradients both for solutes and for biomass components, $S_F(x,y,z)$ and $X_F(x,y,z)$. Moreover, these concentrations are also time dependent as the biofilm continuously develops over time. Biofilm model equations are presented in detail in other publications (Picioareanu et al., 2004; Xavier et al., 2005) therefore only the essential model modifications will be explained here.

Solute components: For any soluble component, a mass balance can be set up by assuming that the transport is only by molecular diffusion and that dissolved components can be produced or consumed in several biotic or abiotic transformation processes with net rate $r_{S,F}$

$$\frac{\partial S_F}{\partial t} = \frac{\partial}{\partial x} \left(D \frac{\partial S_F}{\partial x} \right) + \frac{\partial}{\partial y} \left(D \frac{\partial S_F}{\partial y} \right) + \frac{\partial}{\partial z} \left(D \frac{\partial S_F}{\partial z} \right) + r_{S,F}. \quad (23)$$

Migration of ions in an electrical potential field is here neglected by assuming that the high medium conductivity will make potential gradients insignificant. Eq. (23) is applied on a rectangular computational domain partially filled with biofilm and partially with a mass transfer boundary layer without biofilm. Simplifications are made in 1d and 2d model reductions ($\partial/\partial x$ and/or $\partial/\partial y = 0$). The boundary conditions needed to solve the mass balance Eq. (23) reflect the particular setting of the modeled biofilm system. At $z = L_z$ (top of the biofilm computational domain) bulk concentrations of all soluble components are assumed, $S_F = S_B$. The electrode surface on which the biofilm develops (at $z = 0$) is now

electrochemically active for certain chemical species (e.g., mediators, protons with $r_{S,E} \neq 0$), but inert and impermeable for others ($r_{S,E} = 0$). In general, the boundary condition at the electrode surface expresses the fact that the rate of superficial production of a species on the electrode surface must equal the flux out by diffusion

$$D \frac{\partial S_F}{\partial z} + r_{S,E} = 0. \quad (24)$$

The remaining lateral system boundaries are connected and form a so-called “periodic” boundary type (Picioareanu et al., 2004). The bulk/boundary layer and the boundary layer/biofilm interfaces are considered internal boundaries, where conditions of concentration continuity apply. For the initial state at $t = 0$, a uniform distribution of concentrations throughout the whole domain is assumed, with $S_F = S_B$. The solution of solute mass balances in the biofilm, $S_F(x,y,z)$, at a given moment in time is used to calculate: (i) the overall biofilm reaction rates needed in bulk liquid mass balances (20); (ii) electrode reaction rates and currents because $S_E = S_F(x,y,0)$; (iii) biomass growth rates in the biofilm.

Biomass balances: The model for biomass production/consumption and transport within the biofilm closely follows the individual-based modeling approach (IbM) described and applied in Picioareanu et al. (2004) and Xavier et al. (2005). The relevant parameters are: n_{p0} , initial number of biomass particles, d_x , density of biomass particles, m_0 , initial mass of biomass particles and $m_{x,max}$, critical biomass for biomass particle division (Table 1).

2.2.5. pH calculation

The electrochemical mediator oxidation rate depends on pH, which is in turn altered by both electrode and microbial reactions. The H^+ concentration is calculated from a local charge balance (electroneutrality condition) applied at every location in the biofilm and bulk liquid (Batstone et al., 2002):

$$S_H - \sum_{\text{anions from weak acids}} \left(\frac{K_a S_A}{S_H + K_a} \right) + \sum_{\text{cations from weak bases}} \left(\frac{S_H S_C}{S_H + K_a} \right) - \frac{K_w}{S_H} - \sum_{\text{anions from strong acids}} S_A - \sum_{\text{cations from strong bases}} S_C = 0. \quad (25)$$

The concentrations of anionic species from weak acids, S_{A-} , are expressed from the acidity constant K_a combined with the total concentration of that acid, S_A . A similar treatment is applied for cations from weak bases. Cations from strong bases (e.g., Na^+) or anions from strong acids (e.g., Cl^-) are usually also present. OH^- concentration results from the ionic product of water K_w .

3. Model evaluation: MFC with biofilm and added redox mediator

Several simulations were performed in the standard case conditions (Table 1) and in conditions in which some of the parameters and model assumptions were changed (Table 2).

Table 2 – Summary of model parameters changed in respect to the standard case (Table 1), in all simulated cases

Parameter	Simulation case nos.											Units
	2	3–5	6–8	9	10	11	12,13	14	15	16	17	
	Figure											
	1D-F	6A	6B	7A,B	7C,D	7C,D	7E	7F	8A,B	8A,B,C	8A,B,D	
$S_{0,s}$				100 day	100 days	100 days						gCOD m ⁻³
$S_{0,Mred}$			1									mM
$S_{0,Mox}$			10 ⁻³									mM
D_{Mred}, D_{Mox}					6 × 10 ⁻⁶	6 × 10 ⁻⁶						m ² day ⁻¹
L_L								32				μm
X_0	10	0.25, 2.5, 25	0.25, 2.5, 25	0.25	0.25	0.25						gCOD m ⁻³
n_{p0}		0	0	0	0	0						Particles
R_{ext}							400, 1600					Ω
E_M^0									0.210		0.210	V (SHE)
Y_X									0.068		0.068	(gCOD biomass) (gCOD acetate) ⁻¹
Y_{Mox}, Y_{Mred}									0.058		0.058	(mol mediator) (gCOD acetate) ⁻¹
$q_{Ac,max,XMet}$										10	10	(gCOD acetate) (gCOD biomass) ⁻¹ day ⁻¹
$K_{Ac, Met}$										100	100	gCOD m ⁻³
Y_{XMet}										0.05	0.05	(gCOD biomass) (gCOD acetate) ⁻¹
k_{endo}						0.125						day ⁻¹
$K_{Mox, endo}$						0.1						mM
$Y_{Mox, endo}$						0.0623						(mol mediator) (gCOD biomass) ⁻¹

3.1. Standard case and general characteristics

The main goal for the mathematical model describing the behavior of the microbial fuel cell is to calculate the current produced, as a function of time. Besides, integration of current over time gives the total charge produced. These two characteristics, calculated for the standard case are shown in Fig. 1A. The current increases over a couple of days, in parallel with biomass accumulation both attached on the anode as biofilm and suspended in the liquid phase (Fig. 1B). After about 8 days, the substrate is depleted (Fig. 1C) and, naturally, the total biomass and the biofilm thickness reach a maximum plateau phase (biomass decay has been neglected). The current produced depends on the availability of reduced mediator. When the substrate is depleted, the biomass cannot reduce the oxidized mediator and its concentration in the bulk liquid will gradually decrease (Fig. 1C) due to the fact that M_{Red} is continuously oxidized at the anode. The current reaches its peak when the rate of

substrate consumption is maximum, i.e., the slope of $S_{B,S}$ over time is the steepest. This peak is determined by the balance between all reaction and diffusion rates in the biofilm.

The concentrations S_E at the anode surface can be very different from those in the bulk liquid (S_B). This is due to diffusion limitations, both in the boundary layer and in the biofilm. Because M_{Ox} is formed at the anode surface, $S_{E,Mox} > S_{B,Mox}$ (Fig. 2A) and correspondingly there is less reduced mediator at the electrode than in the bulk (Fig. 2B). The faster the electrochemical conversion of mediator the steeper its concentration profile at the electrode surface. The maximum electrochemical rate (i.e., the maximum current produced) is after about 4 days, when enough biomass has accumulated in the biofilm. However, after day 4 the thicker biofilm causes greater resistance to the mediator and substrate diffusion. Slower diffusion corroborated with lower microbial conversion rates (because substrate concentration decreases, as shown in Fig. 2C) will lead to the gradual fall in current produced. It can be observed from concentration

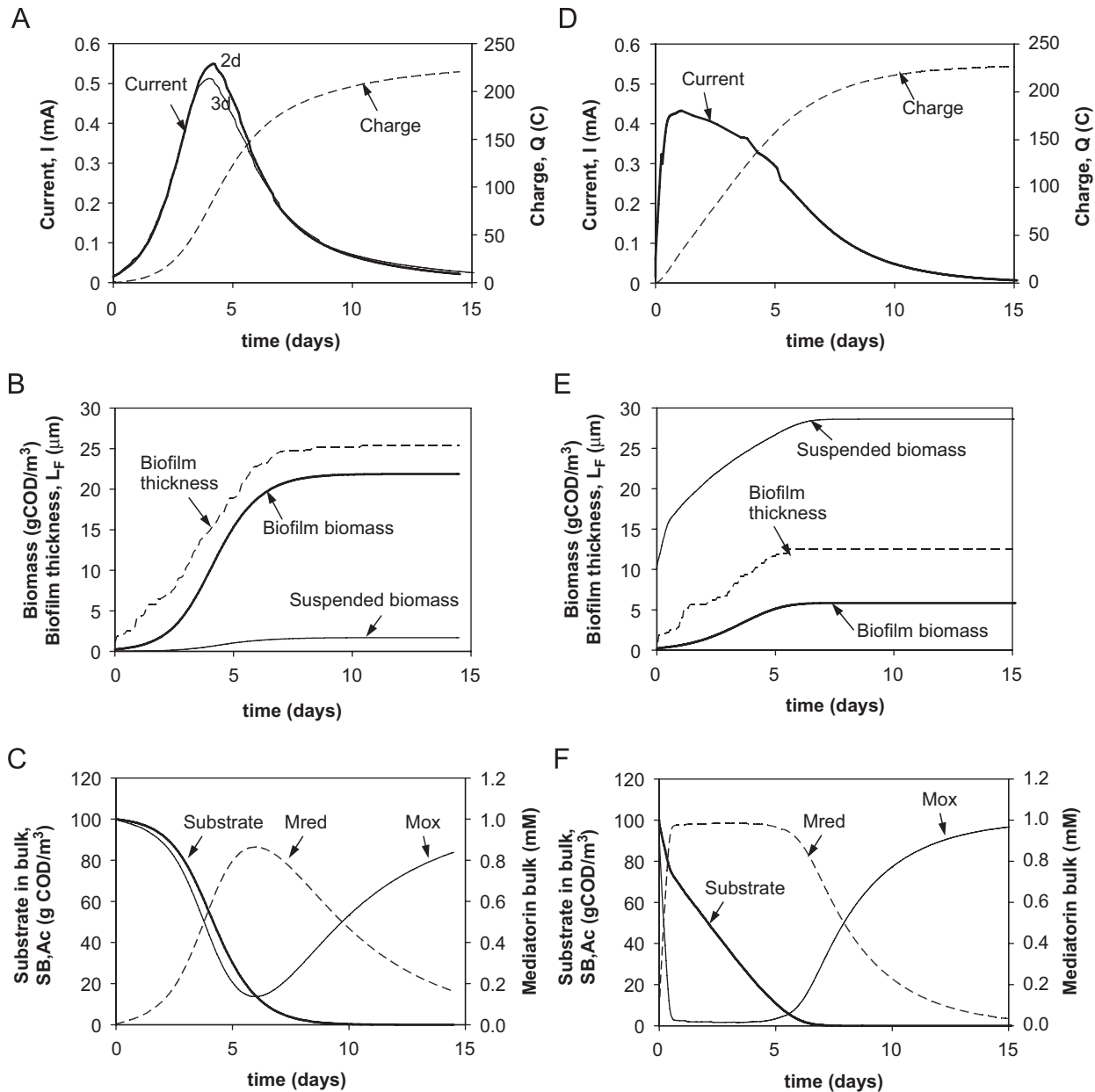


Fig. 1 – Simulated time progress of several MFC process variables: (A–C) in the standard case (parameters in Table 1); (D–F) when starting with much higher concentration of suspended biomass (10 gCOD/m^3 , Table 2, case no. 2). (A and D) electrical parameters (thick line: current in a 2d simulation; thin line: current in a 3d simulation; dashed line: cumulative produced charge); (B and E) biomass-related measures (thick line: concentration of total biofilm biomass per reactor volume; thin line: concentration of suspended biomass per reactor volume; dashed line: maximum biofilm thickness); (C and F) soluble chemical species in bulk liquid (thick line: substrate acetate; thin line: oxidized mediator; dashed line: reduced mediator).

profiles (Figs. 2A and B) that a minimum M_{ox} is correlated with a maximum in M_{red} produced. This is due to the countercurrent diffusion of the electron acceptor (M_{ox}) and donor (acetate) in the biofilm depth. The MFC biofilm system is in this respect similar to the membrane-aerated biofilm used in wastewater treatment, where the electron acceptor (oxygen) diffuses from the membrane side (biofilm support) and the donor (COD or NH_4^+) from the bulk liquid side (Pankhania et al., 1994; Hibiya et al., 2003; Okabe et al., 2004;

Satoh et al., 2004). When the substrate is almost exhausted (for example at day 8), very little microbial conversion occurs in the biofilm but the mediator continues to be oxidized at the anode surface. The absence of microbial conversions correlated with the sink for M_{red} (source for M_{ox}) still present leads to linear concentration profiles, determined only by the rate of diffusion (Fig. 2A and B). Of course, this analysis is valid only in the case where mediator exists in the bulk liquid from the beginning of the MFC run. In the current system the total

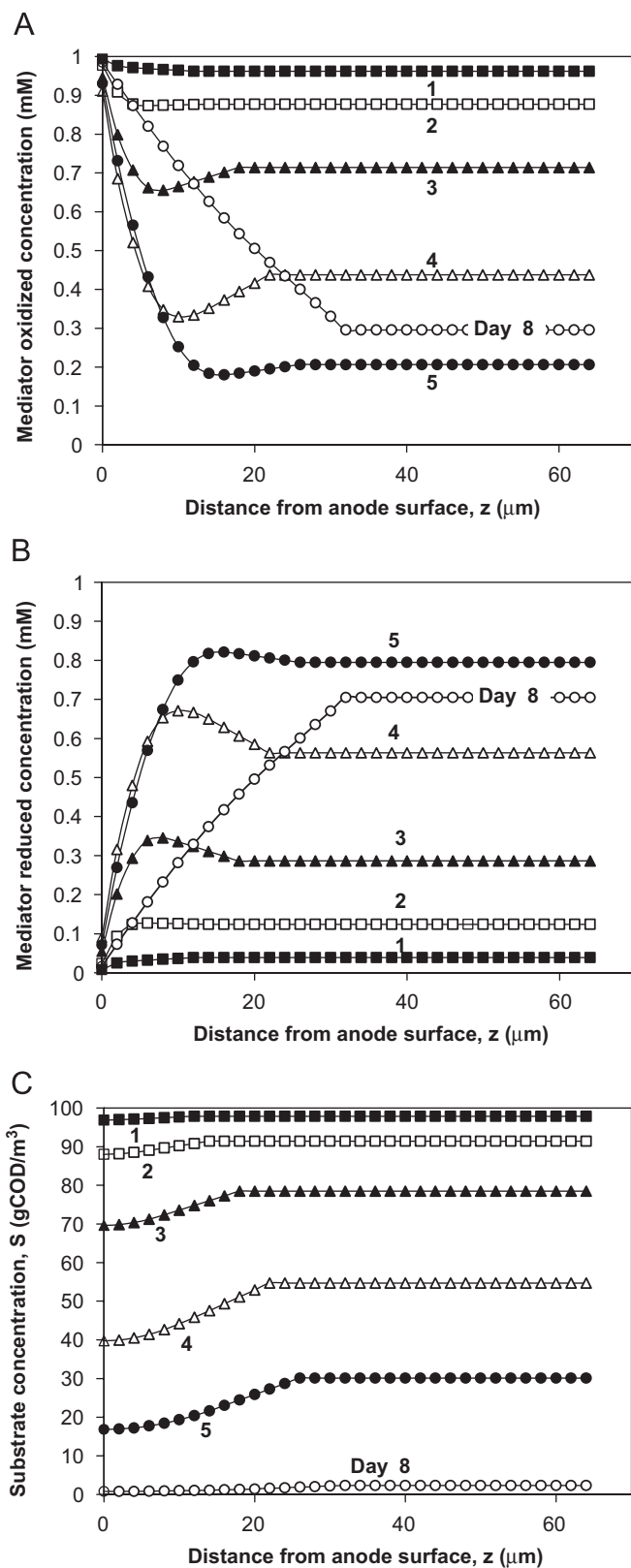


Fig. 2 – Average concentration profiles along the biofilm depth after 1–5 and 8 days, for the MFC biofilm grown in standard conditions: (A) oxidized mediator, \bar{S}_{F,Mo_x} (mM); (B) reduced mediator, $\bar{S}_{F,Mr_{ed}}$ (mM); (C) substrate, $\bar{S}_{F,Ac}$ (gCOD/m³).

amount of mediator is conserved (M_{ox} and M_{red} are merely recycled). If the mediator is produced in-situ by bacteria (Rabaey et al., 2004; Rabaey et al., 2005b) the concentration

profiles and consequently the current generation may be quite different. This interesting aspect should be examined by further modeling studies.

A multidimensional (2d or 3d) model can describe heterogeneous biofilm formation on the anode surface. The effect of a non-uniform biomass distribution on the electrode, calculated by the 2d MFC model, on the current produced can be seen in Fig. 3. The local current density is more intense at places where the electrochemically active bacteria are present (days 1–3 on Fig. 3). In addition, from the distribution of M_{ox} concentration at day 3, radial concentration gradients within a bacterial colony can be seen. This is because M_{ox} is more rapidly consumed at places within colonies where enough substrate is available; this creates a sink towards which the M_{ox} existing in the bulk liquid or formed at the anode will diffuse. If in time the biofilm will cover the whole electrode surface by a homogeneous microbial layer, then uniform current distribution over the electrode is expected (day 6). Moreover, the

concentration gradients will be largely 1d for a flat and homogeneous biofilm, the dominant gradients arising normal to the electrode surface. In this case, while a 2d or 3d model would be needed for young biofilms, a 1d description of the MFC biofilm would be sufficient for the older ones. Formation of biofilm heterogeneity is the concerted action of biomass growth and detachment (Van Loosdrecht et al., 1997), and it has been investigated by several experimental and modeling studies (Kwok et al., 1998; Picioareanu et al., 2004).

The 3d MFC biofilm model produced very similar results (Fig. 4). As in the 2d case, the current distribution over the anode was heterogeneous for younger and patchy biofilms, becoming uniform in older and more homogeneous biofilms. The total current produced in the 3d case was compared with the one in the 2d case (Fig. 1A). The effect of 3d gradients

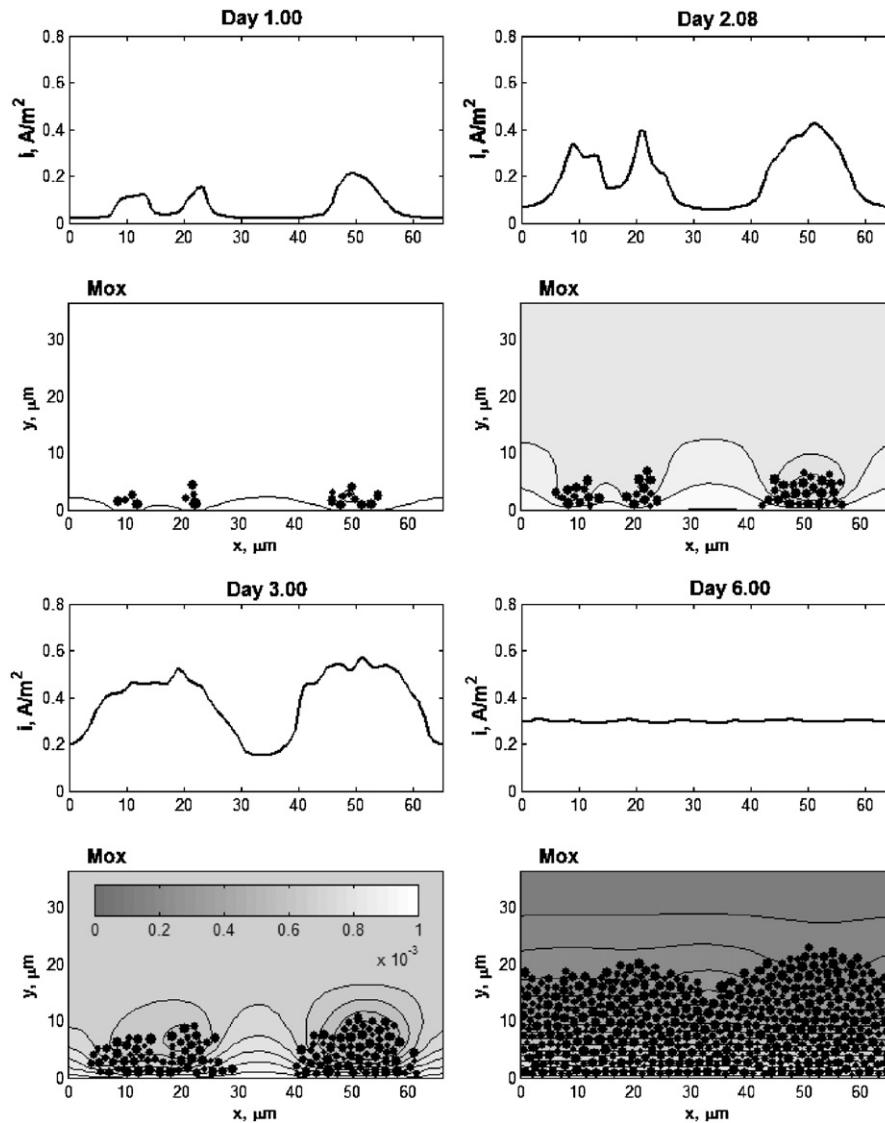


Fig. 3 – Current density i (A/m²) and cells distribution on the anode surface after 1–3 and 6 days, as resulted from a 2d simulation in the standard operation conditions (parameters in Table 1). 2d concentration distributions for the oxidized mediator are shown on the cell distribution plots as gray-scale contour levels. The gray scale used is on the graph at day 3, for concentrations between 0 (minimum, dark gray) and 0.001 M (maximum, white).

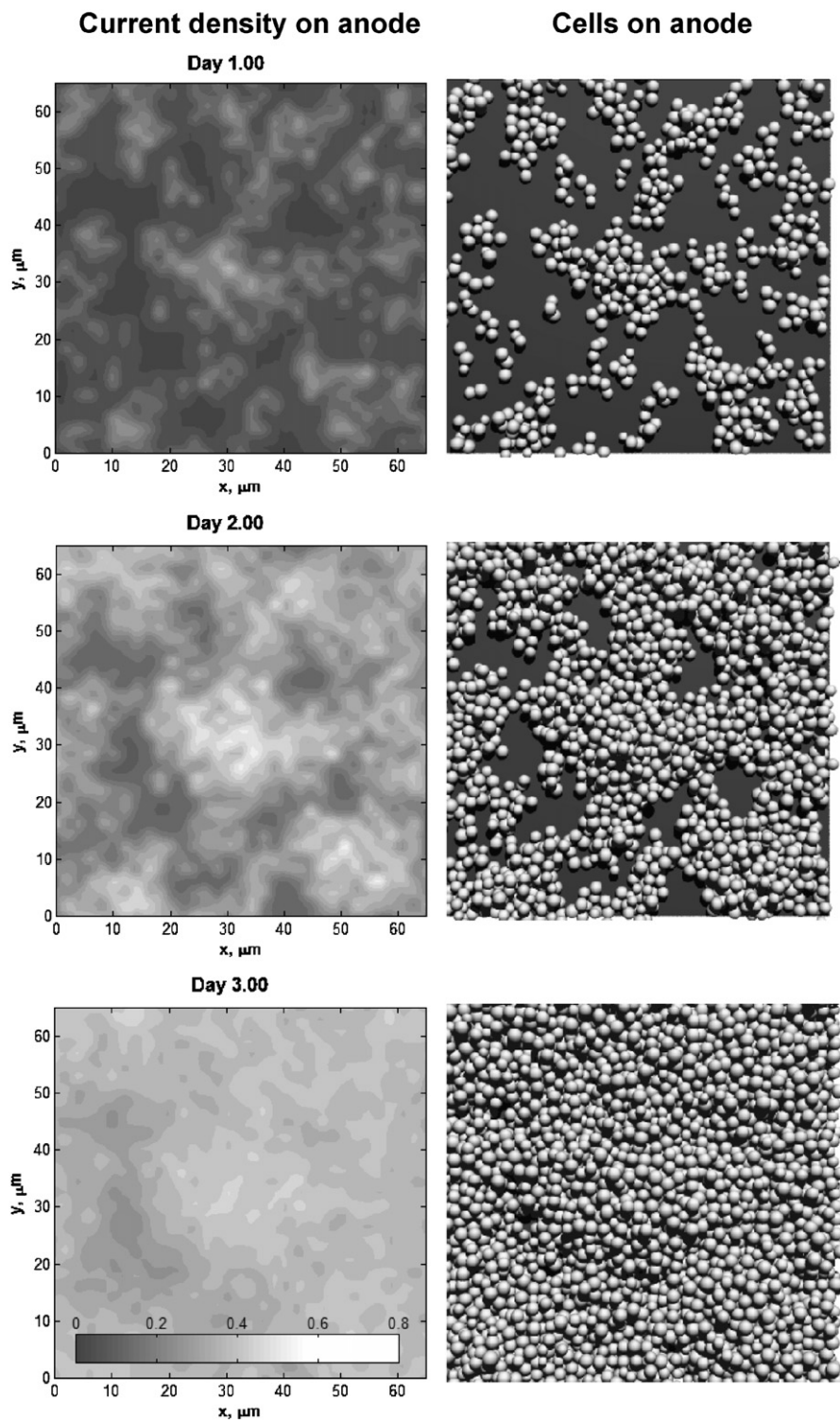


Fig. 4 – Left: current density i (A/m^2); right: cells distribution on the anode surface (view from top) after 1–3 days from a 3d simulation in standard conditions (parameters in Table 1). 2d distributions of current density are shown as gray-scale contour levels. The gray scale used is on the graph at day 3, with i between 0 (minimum, dark gray) and $0.8 A/m^2$ (maximum, white).

seems to be marginal in this case. This again suggests that for rather uniform biofilms 1d or 2d models should give accurate enough descriptions of produced currents. However, for multispecies anode biofilms developing in wastewater fed

MFCs it is likely that more heterogeneous distribution of the electroactive bacteria will occur. 2d and 3d time-dependent models will be invaluable in exploring the effect of such biofilm heterogeneity on MFC performance.

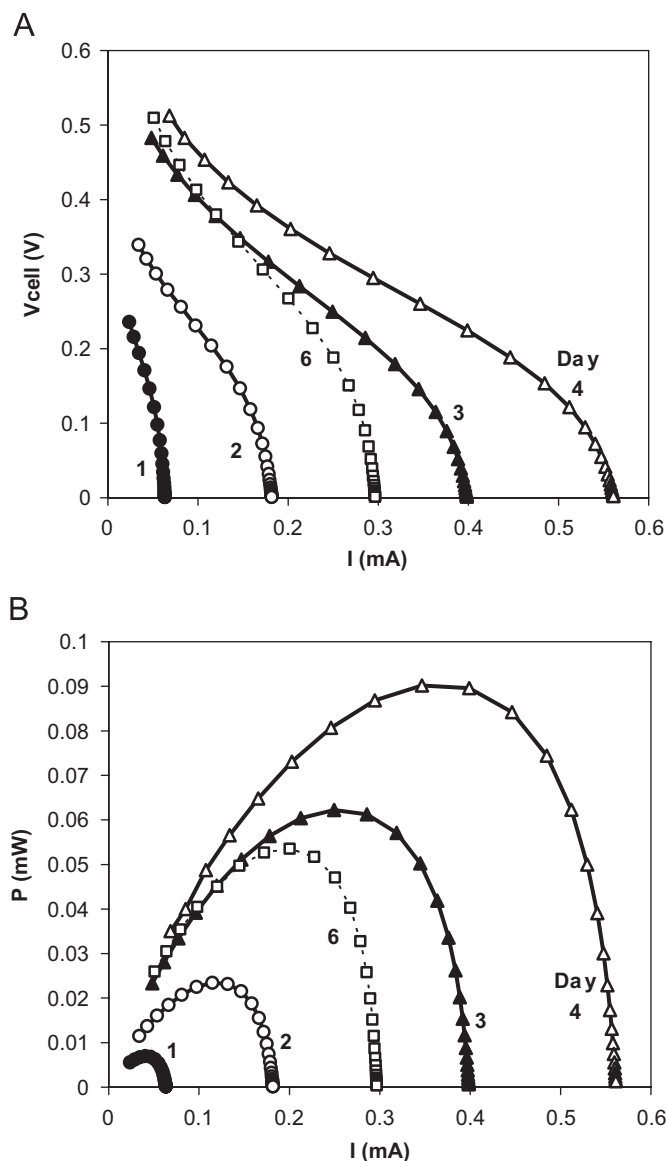


Fig. 5 – Voltage–current (A) and power–current (B) behavior of the MFC simulated in the standard case operation (2d model, parameters in Table 1). The V_{cell} - I and P - I curves are calculated at 1 (black circles), 2 (open circles), 3 (black triangles), 4 (open triangles) and 6 days (open squares) after the start of the MFC run. Each curve is calculated by solving the mass balances for solutes and the total current equation at different resistances R_{ext} , varied from high to low values.

Voltage–current (Fig. 5A) and power–current (Fig. 5B) characteristics can be calculated at different moments in time with the 2d model. From the voltage–current curves, it is clear that the MFC operated with the chosen standard set of parameters functions in a mass-transfer-limited regime (the part of the curves at high currents, Fig. 5A). Diffusion limitations increase by the day, as biofilms get thicker. These outputs of the model are very similar to the characteristic voltage–current and voltage–power relationships observed in real MFC (Logan et al., 2006).

3.2. Competition between suspended and biofilm cells

Suspended and attached growing cells (case no. 2): Starting the system with higher concentrations of suspended cells (e.g.,

10 gCOD/m^3) will obviously give those an advantage in a batch system. Given the same amount of substrate initially added to the MFC, a thinner biofilm with less biomass will develop (Fig. 1E). However, the current produced will quickly increase from the beginning because sufficient initial biomass exists to quickly reduce the mediator (Fig. 1D), until a quasi steady state in the two mediator concentrations is reached (Fig. 1F). This steady state is the result of a balance between the rates of microbial and electrochemical processes.

Growing suspended cells only: When hypothetically no biofilm is allowed to form on the electrode, the diffusion resistance is very much diminished. This results in faster system dynamics: on one hand the steady-state current is quickly reached, on the other hand the current falls more steeply after substrate depletion (see currents in Fig. 6 in comparison

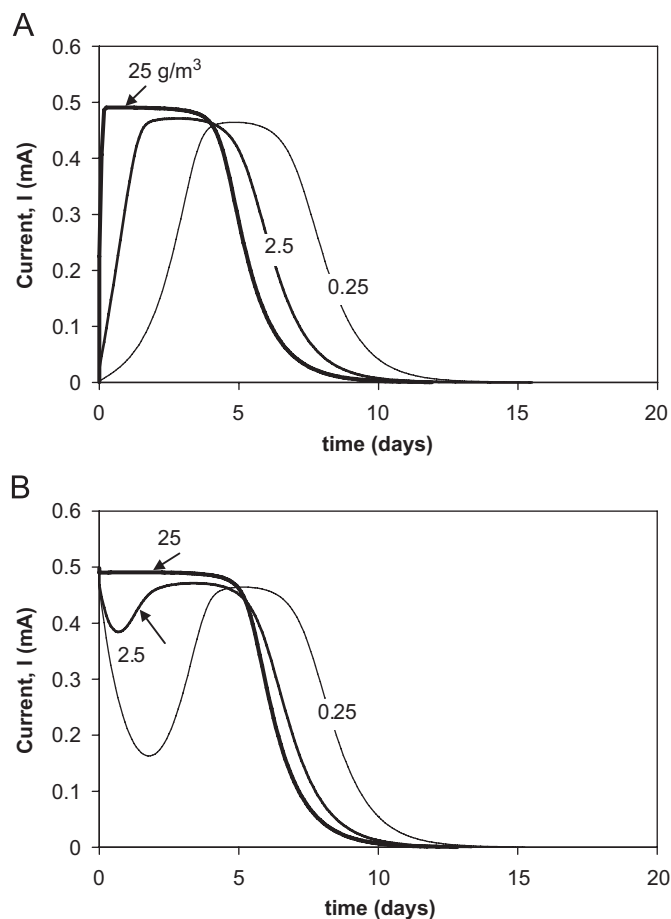


Fig. 6 – Simulated current production in time when only suspended cells are growing in the bulk liquid and no biofilm formation possible. (A) initial biomass concentration $X_0 = 0.25, 2.5$ and 25 gCOD/m^3 , mediator initially in oxidized form ($S_{0,\text{Mred}} = 1 \mu\text{M}$, $S_{0,\text{Mox}} = 1 \text{ mM}$); (B) initial biomass concentration $X_0 = 0.25, 2.5$ and 25 gCOD/m^3 , mediator initially in the reduced form ($S_{0,\text{Mred}} = 1 \text{ mM}$, $S_{0,\text{Mox}} = 1 \mu\text{M}$). Parameters for these simulations are listed in Tables 1 and 2 (A—case nos. 3–5; B—case nos. 6–8).

with those in Fig. 1). The more concentrated the suspended biomass, the faster the system dynamics (Fig. 6A—case nos. 3–5, mediator initially oxidized). If the mediator is initially added in a reduced form (Fig. 6B, case nos. 6–8), the current is already high from the beginning. In the case of low initial biomass concentrations (e.g., 0.25 gCOD/m^3), the current falls until enough biomass is being formed to support the rate of microbial reduction of M_{ox} . Obviously, because no heterogeneous biofilm exists on the planar electrode, a 1d model for mediator diffusion is sufficient in these cases.

Growing suspended cells and repeated additions of substrate: When a new pulse of fresh substrate is added to the MFC after its depletion (case no. 9) the current will very quickly recover to its maximum value and remain constant as long as sufficient substrate is present (Fig. 7A). Due to microbial growth, the biomass concentration increases and the second pulse of substrate is consumed faster than the initial load (Fig. 7B). However, the diffusion of mediator is limiting the current production, and regardless the biomass concentration, the maximum current obtained at the second pulse is still the same as the initial one.

Mediator diffusivity: A higher diffusivity of mediator species (e.g., $6 \times 10^{-6} \text{ m}^2/\text{day}$ in case nos. 10 and 11) means faster mass transfer through the boundary layer, which will speed up the electrochemical reactions. Thus, a higher peak current (0.8 vs. 0.5 mA) can be obtained in this case and the substrate is consumed quicker (compare Fig. 7C with 7A for currents, and Fig. 7D with 7B for substrate). Also, after the first acetate pulse the current attains higher values ($\sim 1.1 \text{ mA}$) because there is more biomass. However, after the second acetate pulse, even with an increased biomass concentration, the peak current does not increase further because mediator transport again becomes limiting.

Endogenous metabolism: Many experimental studies report non-zero currents after the main substrate is exhausted. The straightforward way to represent these observations is by assuming an endogenous metabolism by which the microbial population continues to reduce mediator based on internal biomass reserves of substrate (case no. 11 in Fig. 7C). If endogenous metabolism runs in parallel with the biomass growth supported by substrate availability, then when substrate is finished (between the pulses), the biomass

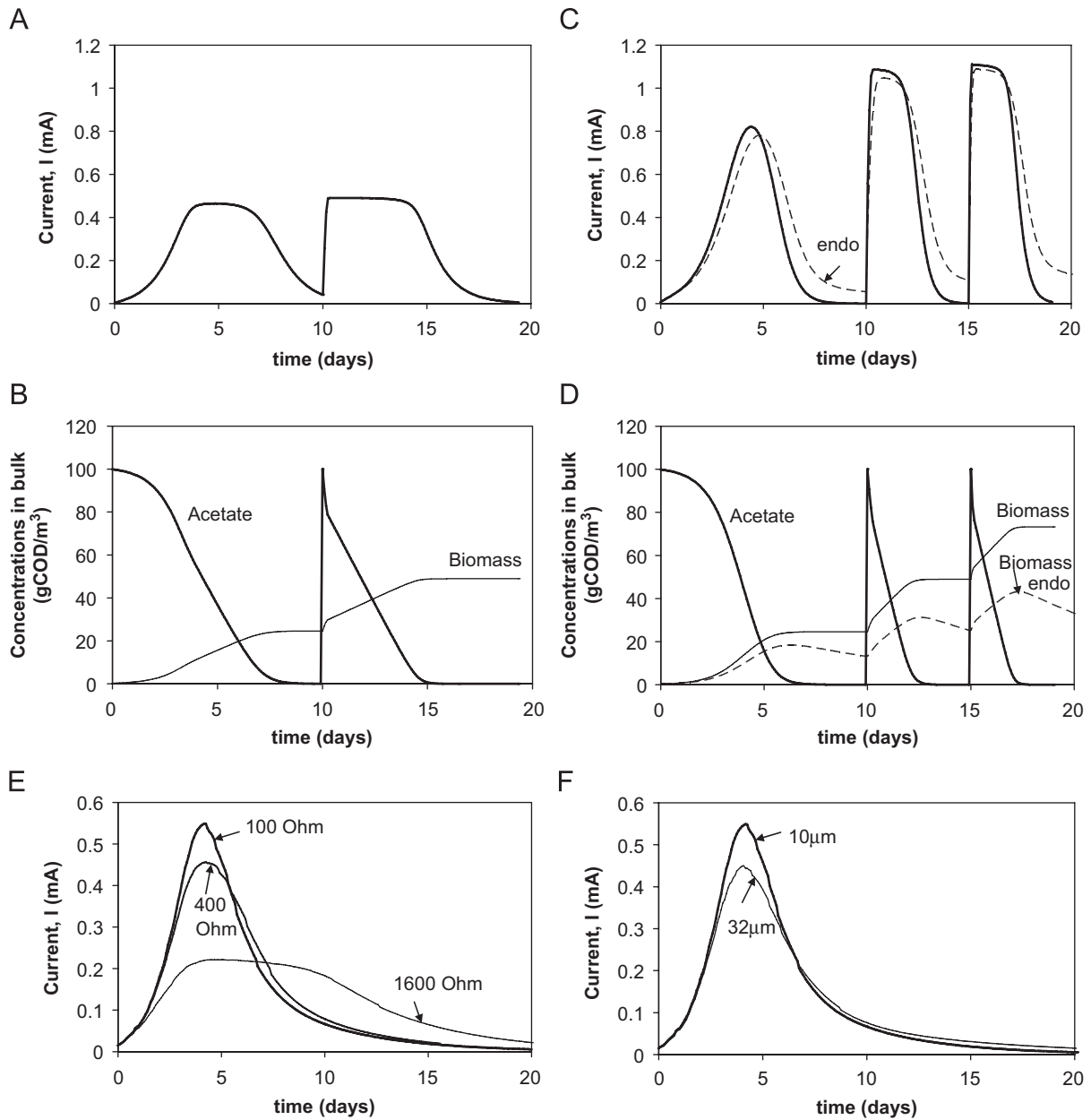


Fig. 7 – (A–D) Simulated current production in time with repeated addition of substrate, when only suspended cells ($X_0 = 0.25 \text{ gCOD/m}^3$) are growing in the bulk liquid and no biofilm formation is possible. (A and B) standard conditions and additional 100 gCOD/m^3 acetate added at day 10: (A) current produced, (B) acetate (thick line) and biomass (thin line) concentrations in the bulk liquid. (C and D) higher diffusivity of mediator ($D_{Mred} = D_{Mox} = 6 \times 10^{-6} \text{ m}^2/\text{day}$), and endogenous metabolism, with 100 gCOD/m^3 acetate added at days 10 and 15: (C) current produced (thick line—standard; dashed line—with endogenous metabolism), (D) acetate (thick line) and biomass (thin line—standard; dashed line—with endogenous metabolism) concentrations in the bulk liquid. (E) Current production in time when the MFC is operated at different external resistor load ($R_{ext} = 100, 400$ and 1600Ω). (F) Influence of external mass transfer resistance ($L_L = 10$ and $32 \mu\text{m}$) on the current production. Parameters for these simulations are listed in Tables 1 and 2 (A and B—case no. 9; C and D—case nos. 10 and 11; E—case nos. 1, 12 and 13; F—case nos. 1 and 14).

concentration will decrease (Fig. 7D). In consequence, the current peaks are smaller (Fig. 7C) but the overall charge produced is larger because also the internally stored reduced material (from before the experiment initiation) is available.

3.3. Electrical resistance and mass transfer resistance

Both increasing the MFC resistance (internal/external from 100 to 400 and 1600Ω —case nos. 12 and 13) and the mass transfer resistance (diffusion boundary layer from 10 to

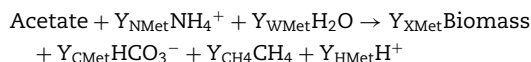
32 μm —case no. 14) have the same effect. The current will decrease at higher resistances, but it will be sustained over longer time periods (Fig. 7E and F) because also the substrate will be consumed more slowly.

3.4. Microbial competition in the biofilm and mediator standard potential

All cases evaluated so far contained a single-species biofilm. However, in all natural environments and in particular in a MFC fed with wastewater mixed microbial populations will cohabit the biofilm. The process of selection of electroactive bacteria on the anodic biofilm would be especially interesting to study. The computational framework presented here is very flexible, so that a model with any number of different microbial metabolic types can be immediately constructed.

To keep the analysis relatively simple, and for illustration of model capabilities only, we assume that acetate can feed two competing microbial populations independently. The first relies for growth on the energy gained by acetate oxidation with mediator. These will be termed electroactive bacteria (EAB) and their growth parameters are given in Table 1. The second is a methanogenic community, which transforms

acetate into methane according to the stoichiometric equation:



and with a rate assumed here to depend only on the acetate concentration

$$\rho_{\text{Met}} = q_{\text{Ac,max,Met}} X_{\text{Met}} \frac{S_{\text{Ac}}}{K_{\text{Ac,Met}} + S_{\text{Ac}}}$$

The parameters for the methanogen community are given in Table 2, case nos. 16 and 17. The contributions of ammonium and water are, like in the case of EAB, neglected.

Results of the model simulations are presented in Fig. 8. When the standard potential of the redox mediator is 0.477 V (SHE), the EAB have a higher growth rate and out compete the methanogens in the biofilm (case no. 16, Fig. 8A and C). Less current and charge will be produced because little part of the acetate is also converted into methane. Because we are interested in the Coulombic yield of acetate conversion, we need to correct the total amount of charge produced by subtracting the contribution due to mediator (which is 48.2 C for the 1 mM mediator initially added). The final Y_Q calculated in this way is 52% compared to 59% in case no. 1.

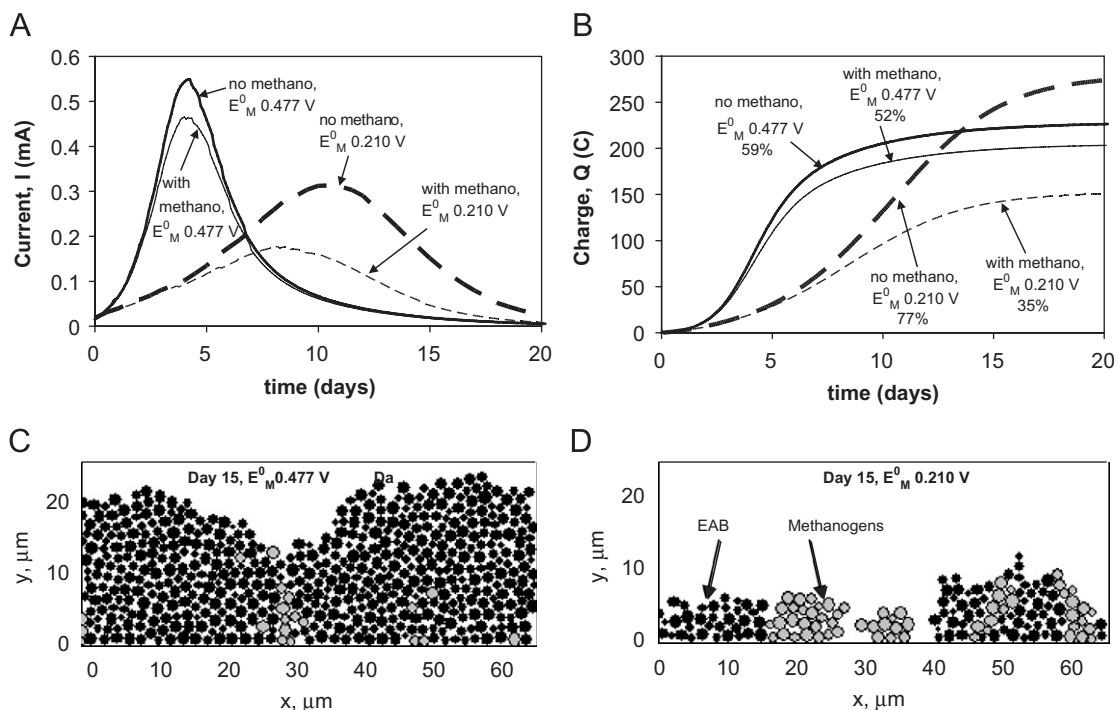


Fig. 8 – (A) Current production in time for the standard case (thick solid line) compared with cases when methanogenic bacteria are competing with the electroactive bacteria, EAB (thin solid line), and when EAB use mediator with a lower standard redox potential, 0.210 V (SHE) (thick dashed line—standard case; thin dashed line—with methanogens). (B) Integral charge produced in time for the four cases in (A). The final coulombic yields in each case are indicated in percentages. Example of 2d distribution of bacteria after 15 days, using mediator with: (C) $E_M^0 = 0.477$ V and (D) $E_M^0 = 0.210$ V. The black circles are the electroactive bacteria and the gray circles the methanogens. Parameters are from Table 1 and 2 (A and B—case nos. 1, 15–17; C—case no. 16; D—case no. 17).

A mediator with lower redox potential, 0.210 V (SHE) in this case, will yield less EAB biomass, as described in the stoichiometry paragraph (Eq. (17)). If less of the available electrons in acetate are used for biomass production, more can be transformed into current. In the absence of methanogens, a higher Coulombic yield (77%) can also be obtained since none of the electrons from acetate oxidation are converted to methane, as in case no. 15 (Table 2 and Fig. 8A and B). However, with methanogens competing for substrate (case no. 17), less current and charge are produced ($Y_Q = 35\%$, Fig. 8A and B). The biofilm is thinner because the overall microbial growth rate is slower, but now it contains a significant fraction of methanogens (Fig. 8D).

4. Model application: comparison model results vs. experimental data

4.1. Case definition

Several types of MFC based on the ability of attached cells within biofilms to transfer electrons to the anode are described in literature. However, the mechanisms of electron transfer to electrodes are not completely elucidated. There are reports of MFC with electron transfer mediated by redox compounds, either artificially added (e.g., Roller et al., 1984) or produced in-situ by bacteria (e.g., Rabaey et al., 2004, 2005a, b) and with electron transfer in the absence of any detected redox mediator (e.g., Bond and Lovley, 2003). Much of this valuable experimental work though does not report essential

data or operational conditions needed as input in a rigorously mechanistic computational model. We have chosen to interpret the MFC system reported by Bond and Lovley (2003) because of its accurate experimental description and availability of essential model parameters. The work was performed with *Geobacter sulfurreducens* and experiments convincingly show that electron-mediating compounds are not likely to play a role in this system. However, some of the conclusions from Bond and Lovley (2003) can be evaluated in the framework of our mathematical model.

Biofilm growth and the associated current production were studied under well-defined conditions in which the effects of electron transfer reactions at the cathode were removed by using a potentiostat to fix the anode at a constant potential (+200 mV versus an Ag/AgCl reference electrode). The model structure is largely the same as in the standard case presented in Section 3. Some model parameters however had to be adapted to reflect the particular system used in Bond and Lovley (2003). These modified parameters and their justification are listed in Table 3.

4.2. Case results and discussion

Acetate (1 mM) was provided with the initial inoculum, and two pulses of 1 mM acetate were given after 4 and 5 days to demonstrate the acetate-dependent growth. When current data extracted from Fig. 3 in Bond and Lovley (2003) are compared with simulation results, a good description of the current produced from the initial acetate medium is apparent

Table 3 – Model parameters changed in respect to the standard case simulation (Table 1) for simulations of biofilm developing on the poised anode of a MFC, according to Bond and Lovley (2003)

Parameter	Description	Value	Units
$S_{0,Ac}$	Initial concentration substrate (acetate) ^a	64 (= 1 mM)	gCOD m ⁻³
D_{Mred}, D_{Mox}	Diffusion coefficient mediator ^b	5×10^{-6}	m ² day ⁻¹
L_L	Mass transfer boundary layer thickness	5	μm
n_{p0}	Initial number of biomass particles	8	Particles
V_B	Bulk liquid volume ^a	2.25×10^{-4}	m ³
A_F	Anode surface area ^a	61.2×10^{-4}	m ²
V_C	Cathode potential ^c	0.4	V (SHE)
$R_{int}+R_{ext}$	Total cell resistance ^c	0	Ω
$i_{0,ref}$	Exchange current density for mediator oxidation in reference conditions ($S_{ref,Mred} = S_{ref,Mox} = 1 \text{ mM}$, $S_{ref,H+} = 10^{-7} \text{ M}$)	0.4	A m ⁻²
E_M^0	Standard reduction potential for the mediator couple (vs. SHE) ^d	0.21	V (SHE)
K_{Ac}	Monod half-saturation coefficient for substrate acetate ^e	1	gCOD m ⁻³
K_{Mox}	Monod half-saturation coefficient for oxidized mediator	0.2	mM
Y_X	Yield biomass on substrate ^f	0.068	(gCOD biomass) (gCOD acetate) ⁻¹
Y_{Mox}, Y_{Mred}	Yield mediator vs. substrate ^f	0.058	(mol mediator) (gCOD acetate) ⁻¹

^a From Bond and Lovley (2003).

^b Increased to enhance the mediator oxidation rate through thicker biofilms.

^c Adapted to work at poised potential of anode (200 mV vs. Ag/AgCl = ~400 mV vs. SHE).

^d Adapted to produce the lower biomass yield needed for reaching a smaller biofilm thickness.

^e Decreased to account for the observed higher affinity of *Geobacter* for acetate.

^f Calculated from a thermodynamic approach based on Heijnen (1999).

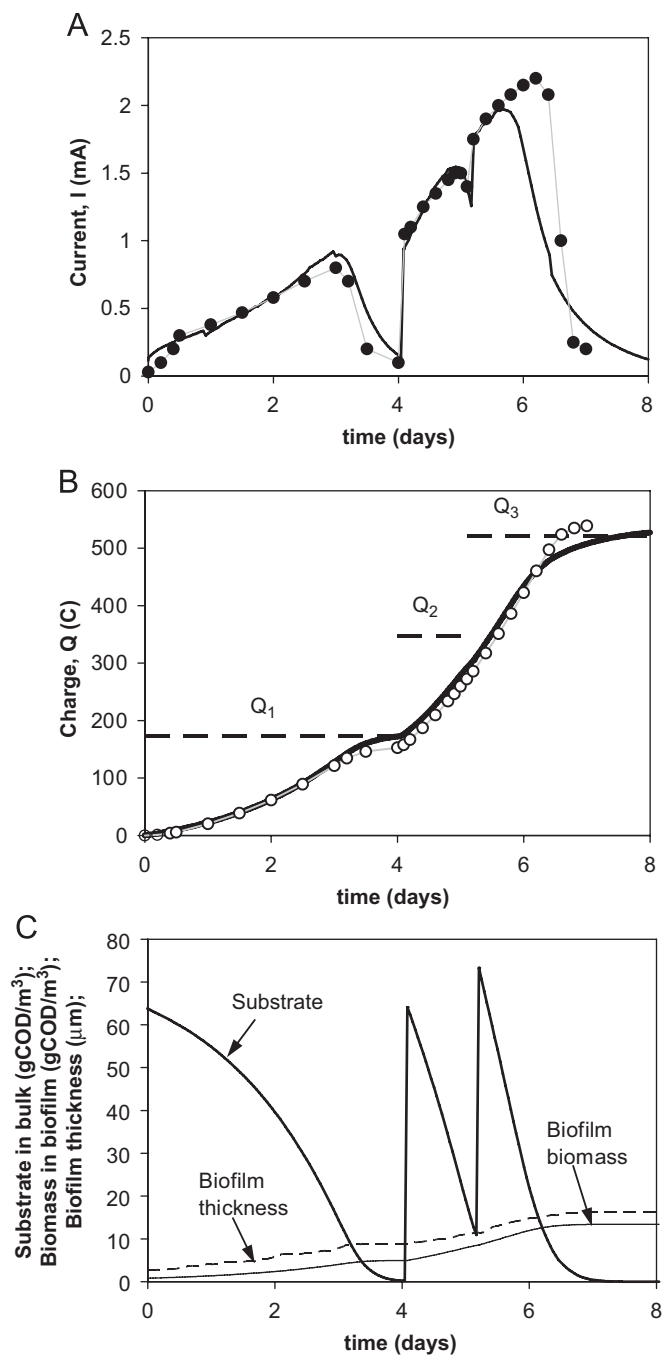


Fig. 9 – Simulation results of a MFC with *Geobacter sulfurreducens* biofilm fed initially with 1 mM acetate and with two subsequent acetate growth medium additions (each of 1 mM). (A) Modeled current production (solid line) and experimental data (black circles) extracted from Fig. 3 from Bond and Lovley (2003). (B) Modeled charge production (solid line) and charge obtained by integration of the current experimentally measured (open circles). (C) Simulated time evolution of bulk substrate concentration (thick solid line), total biofilm biomass (thin line) and biofilm thickness (dashed line). All simulation results are obtained with parameters from Table 3.

(Fig. 9A). The current after the first acetate pulse (4 days) is also correctly described by the model. At the same time, the total amount of charge generated in the experimental setup was calculated by integrating the current produced. Again, the model suitably reproduces the charge produced (Fig. 9B). However, at the second acetate pulse (5 days) the model

predictions begin to deviate from the data obtained experimentally. The simulated current does not reach the peak experimentally observed and starts decreasing sooner than acetate is depleted. This current trend can be easily explained in view of an increased diffusion limitation induced by a thicker biofilm. As the biofilm thickness increases with each

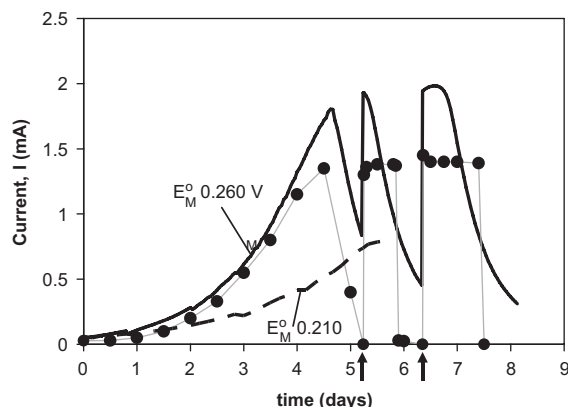


Fig. 10 – Current production in a MFC with *Geobacter sulfurreducens* biofilm, fed initially with acetate (2 mM) and with two medium replacements (acetate 0.5 and 1 mM, no growth factors) at times indicated by the arrows. Experimental data (black circles) were extracted from Fig. 4 from Bond and Lovley (2003). Simulation results are with unchanged parameters from Table 3 (dashed line) and with the mediator potential altered to 0.260 V (solid line).

pulse of acetate (Fig. 9C), the reduced mediator will have increasing difficulty to reach the electrode (and the oxidized mediator to diffuse out of the biofilm). Consequently, the smaller $S_{E,Mred}/S_{E,Mox}$ ratio at the anode will have the effect of decreasing the rate of current production (cf. Eq. (3)). Although the same total amount of charge is produced after all acetate additions (Q_1 , Q_2 and Q_3 on Fig. 9B), the final value (Q_3) is reached more slowly.

An attempt to reproduce by simulations a second set of results (data from Fig. 4 in Bond and Lovley (2003)) is presented in Fig. 10. In this case, the initial acetate concentration was 2 mM and two pulses of acetate (0.5 and 1 mM) were added after removing the growth medium and replacing it with an anaerobic buffer. Because of the non-growth nature of the replaced medium, the instantaneous current does not increase (Fig. 10). Replacing the medium will have the effect of removing the mediator from the bulk liquid. Even with the model assumption that mediator is either still present in the bulk, or produced by cells or present in the biofilm matrix, the experimental data is not well described by the present model. The discrepancy is that, shortly after the current increase following the subsequent acetate additions, the model predicts a decreasing current, in contrast with experiments showing rather constant current levels. Moreover, according to the experiments, after acetate depletion the current should immediately fall to almost zero. The model predicts that the current should only slowly fall to zero as a result of limitations to mediator diffusion in thicker biofilms. Therefore, to explain the experimental data within the framework of the present model one would require either: (i) a thinner biofilm, but this is not consistent with the amount of biomass reported in Bond and Lovley (2003); (ii) larger diffusion coefficients for mediator species, but this

would be unrealistic given the rather large size of the mediator molecules; (iii) a dominant contribution of suspended cells to the current produced (e.g., like in Fig. 7C). This last possibility is ruled out because the medium was replaced with buffer in the experiments. The discrepancy between the experimental results and the output from the simulations might however be explained by differences in the assumed electron transfer mechanism in the model (redox mediator) compared with that operating in the *Geobacter* fuel cell (direct transfer to the anode).

When the parameter set used in this simulation was exactly the same as in Table 3, the current produced was too low (dashed line in Fig. 10) and the coulombic yield different from the experimental one. A better (but still not perfect) fit between the model and the energetic yield data could be obtained increasing E_M^0 from 0.210 to 0.260 V (SHE), which gives $Y_{XS} = 0.107$ gCOD biomass/gCOD acetate. It has to be noted here that the stoichiometry calculations presented in the model description are just an estimation of real yields, based on empirical correlations for the Gibbs energy dissipation (Heijnen, 1999). Moreover, the energy that bacteria need for maintenance has been neglected, which means that the maximum biomass yields were calculated. Finally, standard biochemical conditions were assumed. The environment in a biofilm is not homogeneous, and large concentration gradients can exist. Variable stoichiometry, calculated with Gibbs energies at the local conditions may offer more accurate results, but at increased computational expenses.

In conclusion, it seems reasonable to assume that the electron transfer to the anode in the *Geobacter*-based MFC is less likely to occur by dissolved redox mediators. Further model extensions will have to take into account the possibility of direct electron transfer.

5. Conclusions

The MFC model based on soluble redox mediators and biofilms attached on the anode can realistically describe a series of experimental observations. In order to truly check the plausibility of different computational models for MFC, there is still a need for experiments under more defined conditions. Essential MFC parameters such as internal cell resistances, membrane permeability to different ions or cathodic rates must also be measured and reported. At the same time however, to be of practical use, the general modeling framework presented here must be applied to a more complex case of MFC fed with wastewater containing a mixture of substrates. In this case, the biofilm consists of a complex microbial community, performing a complex network of biochemical transformations. Whereas the global mass balancing and physics equations are known and well-developed components of the model, the bottlenecks are now in: (i) the metabolic description of microbial processes, (ii) the mechanisms of electron transfer to electrode and (iii) differences in electron transfer efficiency in different organisms and consequently the effect of anode microbial community composition. These are areas where further research should be oriented.

Acknowledgments

This research was supported by the European Union through Marie Curie Transfer of Knowledge fellowships to Cristian Picioreanu, and Krishna Katuri through contract number MTKD-CT-2004-517215.

Appendix A. Supporting Material

The online version of this article contains additional supplementary material on model solution and algorithms. Additional data obtained from model runs and animations of simulated biofilm development over time can be obtained from: <http://www.biofilms.bt.tudelft.nl/MFCmodel/index.html>.

REFERENCES

- Batstone, D.J., Keller, J., Angelidaki, I., Kalyuzhnyi, S.V., Pavlostathis, S.G., Rozzi, A., Sanders, W.T.M., Siegrist, H., Vavilin, V.A., 2002. Anaerobic Digestion Model No. 1 (ADM1), IWA Task Group for Mathematical Modelling of Anaerobic Digestion Processes. IWA Publishing, London.
- Batstone, D.J., Keller, J., Blackall, L.L., 2004. The influence of substrate kinetics on the microbial community structure in granular anaerobic biomass. *Water Res.* 38 (6), 1390–1404.
- Bond, D.R., Lovley, D.R., 2003. Electricity production by *Geobacter sulfurreducens* attached to electrodes. *Appl. Environ. Microb.* 69 (3), 1548–1555.
- Bullen, R.A., Arnot, T.C., Lakemanc, J.B., Walsh, F.C., 2005. Biofuel cells and their development. *Biosens. Bioelectron.* 21 (11), 2015–2045.
- Chang, I.S., Moon, H., Bretschger, O., Jang, J.K., Park, H.I., Neelson, K.H., Kim, B.H., 2006. Electrochemically active bacteria (EAB) and mediator-less microbial fuel cells. *J. Microbiol. Biotechnol.* 16 (2), 163–177.
- Fuel Cell Handbook, 2004. Seventh ed., EG&G Technical Services, Parsons, Inc. for the National Energy Technology Laboratory, <www.netl.doe.gov/seca/pubs/FCHandbook7.pdf>.
- Heijnen, J.J., 1999. Bioenergetics of microbial growth. In: Flickinger, M.C., Drew, S.W. (Eds.), *Encyclopedia of Bioprocess Technology: Fermentation, Biocatalysis, and Bioprocess*. Wiley-Interscience, New York, pp. 267–291.
- Hibiya, K., Terada, A., Tsuneda, S., Hirata, A., 2003. Simultaneous nitrification and denitrification by controlling vertical and horizontal microenvironment in a membrane-aerated biofilm reactor. *J. Biotechnol.* 100, 23–32.
- Katz, E., Shipway, A.N., Wilner, I., 2003. Biochemical fuel cells. In: Vielstich, W., Lamm, A., Gasteiger, H.A. (Eds.), *Handbook of Fuel Cells-Fundamentals, Technology, and Application*. Wiley, Chichester, pp. 355–381.
- Kwok, W.K., Picioreanu, C., Ong, S.L., Van Loosdrecht, M.C.M., Ng, W.J., and Heijnen, J.J., 1998. Influence of biomass production and detachment forces on biofilm structures in a biofilm airlift suspension reactor. *Biotechnol Bioeng* 58 (4), 400–407.
- Liu, H., Logan, B.E., 2004. Electricity generation using an air-cathode single chamber microbial fuel cell in the presence and absence of a proton exchange membrane. *Environ. Sci. Technol.* 38, 4040–4046.
- Logan, B.E., Hamelers, B., Rozendal, R., Schröder, U., Keller, J., Freguia, S., Aelterman, P., Verstraete, W., Rabaey, K., 2006. Microbial fuel cells: methodology and technology. *Environ. Sci. Technol.* 40 (17), 5181–5192.
- Lovley, D.R., 2006. Bug juice: harvesting electricity with microorganisms. *Nat. Rev. Microbiol.* 4, 497–508.
- Menicucci, J., Beyenal, H., Veluchamy, R.A., Demir, G., Lewandowski, Z., 2006. Procedure for determining maximum sustainable power generated by microbial fuel cells. *Environ. Sci. Technol.* 40, 1062–1068.
- Newman, J.S., 1991. *Electrochemical systems*, second ed. Prentice-Hall, Englewood Cliffs, NJ.
- Okabe, S., Kindaichi, T., Ito, T., Satoh, H., 2004. Analysis of size distribution and areal cell density of ammonia-oxidizing bacterial microcolonies in relation to substrate microprofiles in biofilms. *Biotechnol. Bioeng.* 85 (1), 86–95.
- Pankhania, M., Stephenson, T., Semmens, M.J., 1994. Hollow fibre bioreactor for wastewater treatment using bubbleless membrane aeration. *Water Res.* 28 (10), 2233–2236.
- Picioreanu, C., Van Loosdrecht, M.C.M., 2002. A mathematical model for initiation of microbiologically influenced corrosion by differential aeration. *J. Electrochem. Soc.* 149 (6), B211–B223.
- Picioreanu, C., Kreft, J.-U., van Loosdrecht, M.C.M., 2004. Particle-based multidimensional multispecies biofilm model. *Appl. Environ. Microb.* 70 (5), 3024–3040.
- Rabaey, K., Lissens, G., Siciliano, S.D., Verstraete, W., 2003. A microbial biofuel cell capable of converting glucose to electricity at high rate and efficiency. *Biotechnol. Lett.* 25, 1531–1535.
- Rabaey, K., Boon, N., Siciliano, S.D., Verhaege, N., Verstraete, W., 2004. Biofuel cells select for microbial consortia that self-mediate electron transfer. *Appl. Environ. Microb.* 70 (9), 5373–5382.
- Rabaey, K., Verstraete, W., 2005. Microbial fuel cells: novel biotechnology for energy generation. *Trends Biotechnol.* 6, 291–298.
- Rabaey, K., Lissens, G., Verstraete, W., 2005a. Microbial fuel cells: performances and perspectives. In: Lens, P.N., Westermann, P., Haberbauer, M., Moreno, A. (Eds.), *Biofuels for Fuel Cells: Biomass Fermentation Towards Usage in Fuel Cells*.
- Rabaey, K., Boon, N., Höfte, M., Verstraete, W., 2005b. Microbial phenazine production enhances electron transfer in biofuel cells. *Environ. Sci. Technol.* 39, 3401–3408.
- Reguera, G., McCarthy, K.D., Mehta, T., Nicoll, J.S., Tuominen, M.T., Lovley, D.R., 2005. Extracellular electron transfer via microbial nanowires. *Nature* 435 (7045), 1098–1101.
- Roller, S.D., Bennetto, H.P., Delaney, G.M., Mason, J.R., Stirling, J.L., Thurston, C.F., 1984. Electron-transfer coupling in microbial fuel cells. 1. Comparison of redox-mediator reduction rates and respiratory rates of bacteria. *J. Chem. Technol. Biotechnol. B Biotechnol.* 34, 3–12.
- Satoh, H., Ono, H., Rulin, B., Kamo, J., Okabe, S., Fukushi, K.-I., 2004. Macroscale and microscale analyses of nitrification and denitrification in biofilms attached on membrane aerated biofilm reactors. *Water Res.* 38, 1633–1641.
- Schubert, C., 2006. Microbiology: batteries not included—circuits of slime. *Nature* 441 (7091), 277–279.
- Shukla, A.K., Suresh, P., Berchmans, S., Rahjendran, A., 2004. Biological fuel cells and their applications. *Curr. Sci.* 87, 455–468.
- Stams, A.J.M., De Bok, F.A.M., Plugge, C.M., Van Eekert, M.H.A., Dolfin, J., Schraa, G., 2006. Exocellular electron transfer in anaerobic microbial communities. *Environ. Microbiol.* 8 (3), 371–382.
- Van Loosdrecht, M.C.M., Picioreanu, C., Heijnen, J.J., 1997. A more unifying hypothesis for the structure of microbial biofilms. *FEMS Microbiol. Ecol.* 24, 181–183.
- Xavier, J.B., Picioreanu, C., Van Loosdrecht, M.C.M., 2005. A general description of detachment for multidimensional modelling of biofilms. *Biotechnol. Bioeng.* 91 (6), 651–669.
- Zhang, X.-C., Halme, A., 1995. Modeling of a microbial fuel cell process. *Biotechnol. Lett.* 17, 809–814.